

## SUPPLEMENTAL INFORMATION

# Role of Ion-Selective Membranes in the Carbon Balance for CO<sub>2</sub> Electroreduction via Gas Diffusion Electrode Reactor Designs

Ming Ma,<sup>†</sup> Sangkuk Kim,<sup>†</sup> ‡ Ib Chorkendorff<sup>†</sup> and Brian Seger<sup>†,\*</sup>

<sup>†</sup>Surface Physics and Catalysis (Surfcats) Section, Department of Physics, Technical University of Denmark, 2800 Kgs Lyngby, Denmark

<sup>‡</sup>Surface Chemistry Laboratory of Energy/Electronic Materials (SCHEMA), Department of Chemical Engineering, Pohang University of Science and Technology, Pohang 37673, Korea

\*Author to whom correspondence should be addressed.

E-mail address: [brse@fysik.dtu.dk](mailto:brse@fysik.dtu.dk)

Tel.: +45 45253174

## Materials

Potassium bicarbonate ( $\geq 99.95\%$ ) purchased from Sigma Aldrich was used in this study without further purification. Anion exchange membrane (AEM, Fumasep FAA-3-PK-75), cation exchange membrane (Nafion<sup>TM</sup> 212), bipolar membrane (BPM, Fumasep FBM) and gas-diffusion electrode (GDE, Sigracet 39 BC) were purchased from Fuel Cell Store. Iridium dioxide ( $\text{IrO}_2$ ) purchased from Dioxide Materials was used as an anode in flow electrolyzers of high-rate  $\text{CO}_2$  reduction.

## Catalysts preparation

For obtaining high purity Cu catalyts, Cu layers were prepared on top of microporous layer of gas-diffusion electrodes by direct current magnetron sputtering (50 W) from a Cu target at an argon pressure of 2 mTorr. Figure 1S shows a typical schematic illustration for Cu deposition using magnetron sputtering under an argon ambient. The energetic  $\text{Ar}^+$  ions are created in a glow discharge plasma, thus  $\text{Ar}^+$  bombardment occurs on the cathode Cu target, which leads to the removal of Cu atoms. Subsequently, the sputtered Cu atoms condense on a substrate (i.e. GDE) to form a Cu layer. In this work, with  $\sim 4$  nm/min Cu deposition rate, the thickness of the Cu layers were controlled by the deposition time.

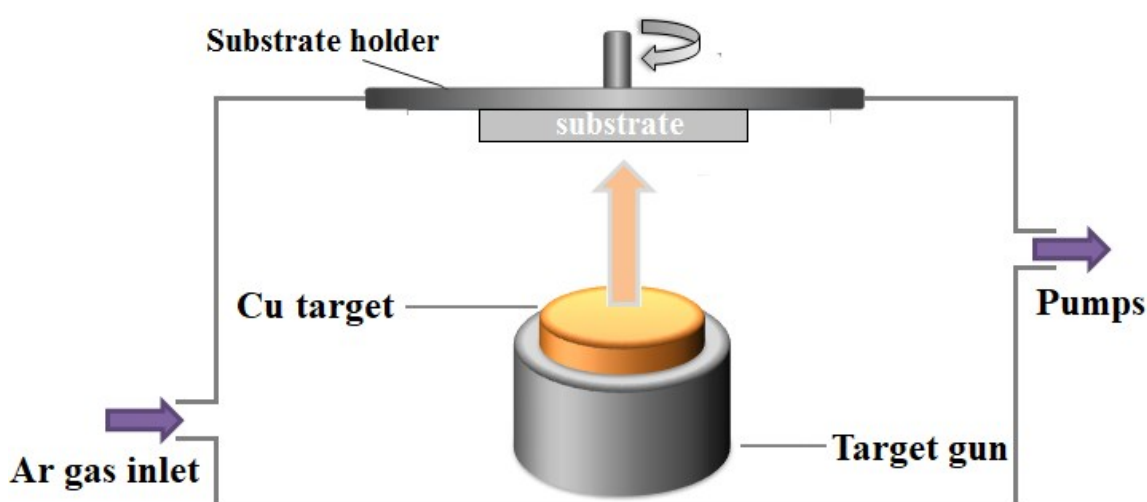
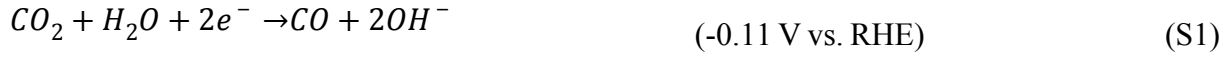


Figure S1. Schematic illustration of magnetron sputtering for Cu deposition from a Cu target.

### High local pH near the cathode

During the process of electrochemical reduction of CO<sub>2</sub>, CO<sub>2</sub> and H<sub>2</sub>O can be electrochemically converted into a variety of gaseous products such as CO, C<sub>2</sub>H<sub>4</sub> and CH<sub>4</sub> on the surface of the catalyst in electrolytes based on the below reactions<sup>1-4</sup>:



In addition to gaseous products, liquid such as ethanol, formate and acetate also can be produced on the surface of the catalyst in aqueous solutions, as follows:



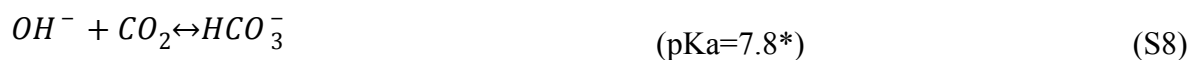
In the electrocatalytic CO<sub>2</sub> reduction process, the competing H<sub>2</sub> evolution is an unavoidable reaction. The electroreduction of H<sub>2</sub>O to H<sub>2</sub> on the surface of catalyst according to the reaction<sup>1</sup>:



Due to the above cathodic reactions (Equation (3-9)), a large amount of OH<sup>-</sup> ions can be created at the cathode/electrolyte interface at high current densities, which creates a significantly higher pH near the surface of cathode compared to that of the bulk solutions.<sup>2,3</sup>

### CO<sub>2</sub> capture via high local pH

During CO<sub>2</sub> reduction in flow electrolyzers using 1 M KHCO<sub>3</sub>, CO<sub>2</sub> from the gas chamber of the electrolyzers reacts with OH<sup>-</sup> ions produced at the cathode/electrolyte interface according to the below reactions of CO<sub>2</sub> and OH<sup>-</sup>:





\* This is at a CO<sub>2</sub> partial pressure of 1 bar in 1 M HCO<sub>3</sub><sup>-</sup>.<sup>5</sup>

### CO<sub>2</sub> reduction performance

The electrocatalytic reduction of CO<sub>2</sub> was performed in a three-chamber flow electrolyzer made from Teflon at ambient temperature and pressure. At the reactor, an ion-selective membrane was used to separate catholyte and anolyte flow compartments. Catholyte and anolyte bottles were filled with 50 ml 1 M KHCO<sub>3</sub>, respectively (Figure S2). In addition, a fixed geometric surface area (2 cm<sup>2</sup>) of Cu layer was used for all the tests in this study.

CO<sub>2</sub> was purged into gas compartment at a constant flowrate of 45 ml/min, and then a fraction of gaseous CO<sub>2</sub> diffuses to the surface of the catalyst in electrolyte for CO<sub>2</sub> conversion. In addition, CO<sub>2</sub> also can be captured to form carbonate (equation S8 and S9) via the reaction of CO<sub>2</sub> with OH<sup>-</sup> generated at the cathode/electrolyte interface.<sup>5</sup> Thus, the high CO<sub>2</sub> conversion rate to gas (C<sub>2</sub>) and liquid products as well as high local pH can lead to a substantial CO<sub>2</sub> consumption at high current densities, correspondingly varying the gas flow (gas mixture) out of the reactor. The volumetric flowrate of gas outlet (gas mixture) after reactor was monitored by flow meter in CO<sub>2</sub> reduction (Figure S2), and then faradaic efficiencies of gas products were evaluated under the consideration of gas flow variation between inlet and outlet. It should be noted that the average catalytic selectivity of gas products during 2.5 h CO<sub>2</sub> reduction electrolysis was used in this work.

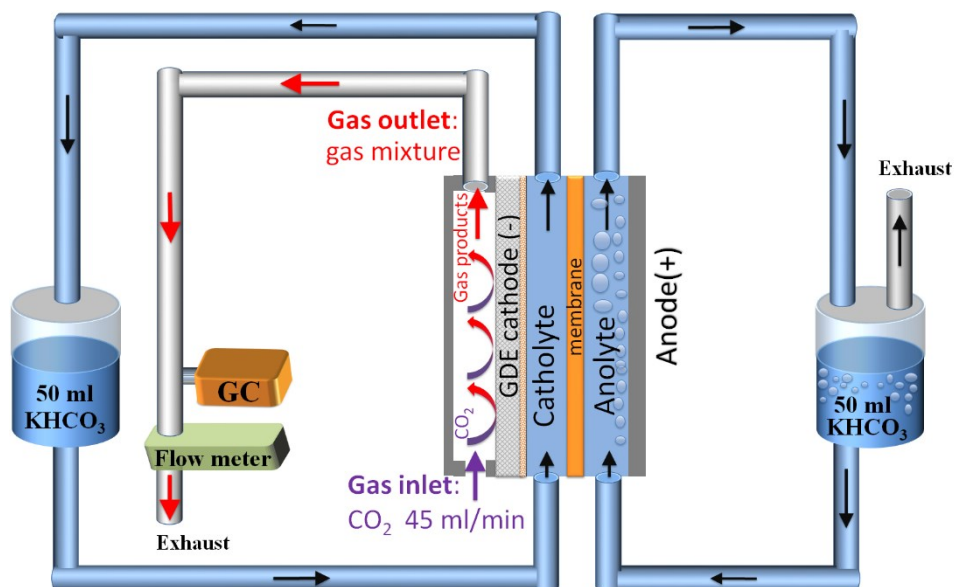


Figure S2. Schematic illustration of flow cell setup for electrocatalytic CO<sub>2</sub> reduction.

### Gas and liquid product analysis

Gas products mixing with unreacted CO<sub>2</sub> flowed out of the electrolyzers, directly injecting into the gas-sampling loop of a gas chromatography (PerkinElmer, Clarus® 590). Ar was used as a carrier gas with a constant flowrate of 10 sccm. The gas chromatography was equipped with a packed Molecular sieve 13x column and a packed Hayesep Q column to separate the gas products. Thus, H<sub>2</sub>, CO, CH<sub>4</sub> and C<sub>2</sub>H<sub>4</sub> could be identified at different reaction times using a thermal conductivity detector. In addition, the peak area of each gas product was compared to standards (calibration gases) to determine the corresponding concentration of gaseous products. Thus, we can get the faradaic efficiency of a certain gas product as follows:

$$FE (\%) = \frac{n \times C_{gas\ product} \times \phi t \times \frac{P_o}{RT} \times F}{I \times t} \times 100\%$$

$$= \frac{n \times C_{gas\ product} \times \phi \times \frac{P_o}{RT} \times F}{I} \times 100\% \quad (S10)$$

where  $n$  is the number of electrons required for producing one molecule of the related gas product, and  $C_{gas\ product}$  is the concentration of gas product measured by GC (here,  $C_{gas\ product}$  is

the mole fraction of gas product in the total gas outlet mixture).  $\phi$  and  $t$  is the gas flowrate out of the electrolyzers and the electrolysis time, respectively.  $P_o$  is the ambient pressure,  $R$  is the ideal gas constant,  $T$  is the absolute temperature,  $F$  is Faraday constant, and  $I$  is the applied current.

The liquid-phase products are analyzed after the electrolysis using a high performance liquid chromatography (HPLC, Agilent 1200 series). Liquid-phase products were separated by an Aminex HPX-87H column (Bio-Rad) that was maintained at 50 °C for the duration of the detection. The HPLC was equipped with a diode array detector (DAD) and a refractive index detector (RID), and the signal response of the DAD and RID was calibrated by known concentration solutions. Thus, we can get the concentration of the detected liquid-phase product. The faradaic efficiency of liquid products can be calculated by equation:

$$FE (\%) = \frac{n \times C_{liquid\ product} \times V \times F}{I \times t} \times 100\% \quad (S11)$$

where  $n$  is the number of electrons required for producing one molecule of the related liquid product, and  $C_{product}$  is the molar concentration of gas product measured by HPLC.  $V$  is the volume of the electrolyte. To obtain accurate selectivity of liquid products, we measured the volume of catholyte and anolyte after electrolysis, respectively.

### Collection of liquid from electrolyte

It should be noted that the ion species carried with water molecules (hydrated ion) transports via membrane, which means the volume of catholyte and anolyte was varied after electrolysis. For AEM, a decrease in catholyte volume was observed with increased anolyte volume after several hours of CO<sub>2</sub> reduction electrolysis, because of the transportation of the anion species hydrated with water molecules from catholyte to anolyte via AEM as charge carriers. In contrast, the use of CEM experienced an increased catholyte volume with correspondingly decreased anolyte over the course of electrolysis, due to that the cation species hydrated water molecules transported from anolyte to catholyte via AEM as charge carriers. Notably, no obvious variation in both catholyte and anolyte when BPM was used, which is due to that water supplied almost equally from both catholyte and anolyte was dissociated into H<sup>+</sup> and OH<sup>-</sup>, transporting to catholyte and anolyte, respectively.

Based on the aforementioned discussion, in order to obtain accurate selectivity of liquid products, volume of catholyte and anolyte was also measured for each test after electrolysis, respectively.

### **Collection of liquid products evaporated from GDEs**

Some liquid products can be evaporated from the gas diffusion layer of GDE and then flow out of the gas compartment of the reactor with unreacted CO<sub>2</sub> and gas products. To collect the evaporated liquid products from GDEs (i.e. gas chamber), gas outlet flow after the reactor was directly purged into a sealed bottle filled with 30 ml de-ionized water (the outlet flow tube was immersed into de-ionized water), as shown in Figure S3. After completion of CO<sub>2</sub> reduction, the liquid products diluted with de-ionized water in that sealed bottle were analysed via high-performance liquid chromatography (HPLC). Figure 2b presents the faradaic efficiencies of liquid products evaporated from GDEs when using distinct ion-selective membranes, indicating that only alcohols products such as ethanol and propanol evaporate and escape from the cathode/electrolyte interface irrespective of membrane types, which is due to their high volatility.

In addition, both catholyte and anolyte in the given reservoirs were collected for quantification of liquid products, owing to liquid products crossover from catholyte to anolyte via membranes.<sup>5</sup> Thus, the total amount of one certain liquid product formed on cathode GEDs can be written as:

$$N_{total\ liquid} = N_{liquid\ in\ anolyte} + N_{liquid\ in\ catholyte} + N_{evaporated\ liquid} \quad (S12)$$

where  $N_{liquid\ in\ anolyte}$  and  $N_{liquid\ in\ catholyte}$  are the amount of one certain liquid product detected in anolyte and catholyte, respectively.  $N_{evaporated\ liquid}$  is the amount of one certain liquid product evaporated from GDEs. Here, the evaporation ratio of one certain liquid product formed on cathode GDEs can be calculated based on the below equation:

$$Evaporation\ ratio\ (\%) = \frac{N_{evaporated\ liquid}}{N_{total\ liquid}} \times 100\% \quad (S13)$$

Thus, the equation (S13) was used to calculate a ratio between the amount of one certain liquid product evaporated from GDEs and the total amount of corresponding liquid product formed on the cathode, as shown in Figure S4.

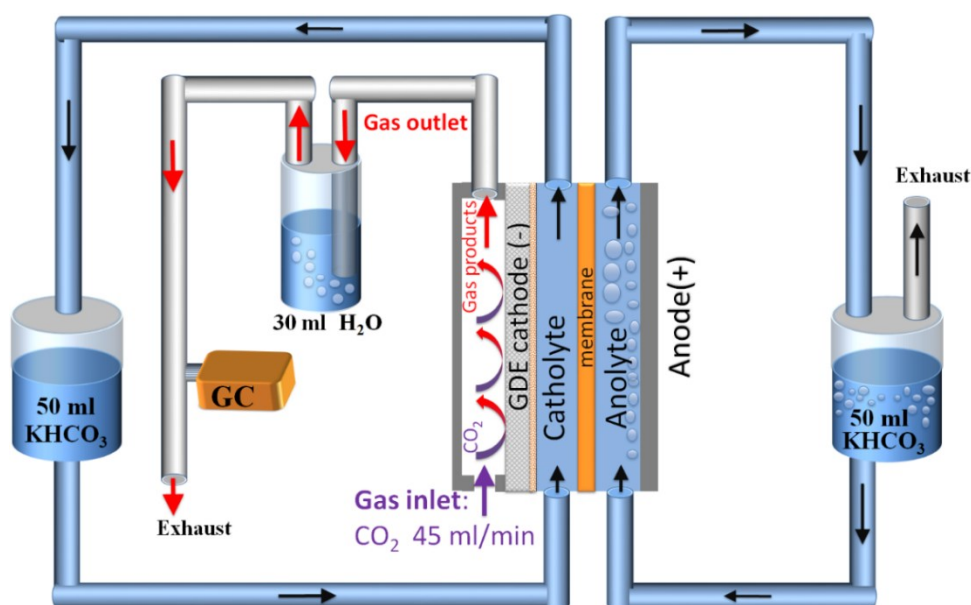


Figure S3. The schematic illustration of flow cell setup for collecting liquid products evaporated from GDEs during CO<sub>2</sub> reduction.



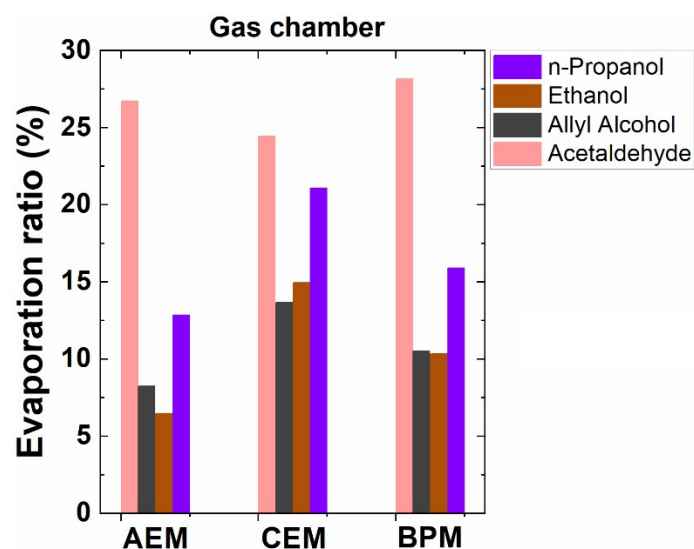


Figure S4. Evaporation ratio of related liquid products escaped from GDEs (i.e. gas chamber) at 200 mA/cm<sup>2</sup> when using AEM, CEM and BPM, respectively.

### Analysis of gas released from the anolyte

When the electrocatalytic CO<sub>2</sub> reduction occurs on the surface of the cathode, water oxidation reaction (i.e. O<sub>2</sub> evolution) takes place on the anode surface. By the water oxidation reaction, a large amount of H<sup>+</sup> can be created at the anode/electrolyte interface, which leads to a decrease of pH locally near the anode. Subsequently, H<sup>+</sup> produced at the anode/electrolyte interface can be neutralized with HCO<sub>3</sub><sup>-</sup>, CO<sub>3</sub><sup>2-</sup> or OH<sup>-</sup> in anolyte. The H<sup>+</sup> neutralization with HCO<sub>3</sub><sup>-</sup> or CO<sub>3</sub><sup>2-</sup> forms CO<sub>2</sub>, leading to CO<sub>2</sub> degassing from anolyte with the stream of O<sub>2</sub>.<sup>5</sup> For analysing the gases released from anolyte over the course of CO<sub>2</sub> reduction, the flow electrolyser setup in Figure S5 was utilized. In that setup, N<sub>2</sub> at a constant flowrate was used as a carrier, thus gases released from anolyte were diluted with N<sub>2</sub>, directly venting into the gas sampling-loop of the GC for periodical quantification. The volumetric gas flow released from anolyte was also monitored by in situ flow meter over the electrolysis, as shown in Figure S5.

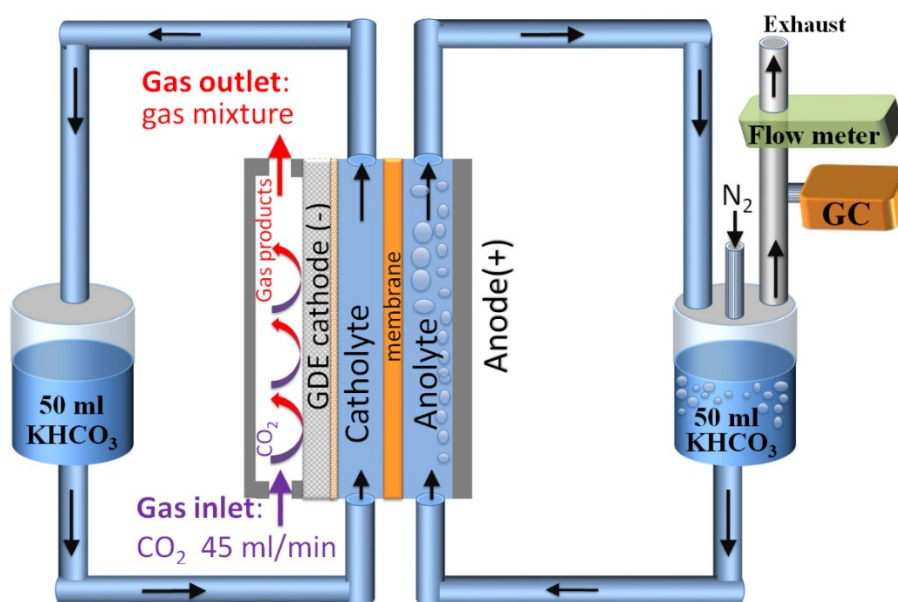


Figure S5. The schematic illustration of flow cell setup for detection of gases released from the anolyte over the course of CO<sub>2</sub> reduction.

### Analysis of gas released from the catholyte using BPMs

No any gas evolution in catholyte was observed when AEM or CEM was used. However, under the use of bipolar membrane in flow electrolyzers, we found that gas bubbles released from the catholyte, which is unique in comparison with the other two membranes. To analyze the gas released from catholyte over the course of CO<sub>2</sub> reduction using BPM, a test setup in Figure S6 was utilized. Similar to gas analysis from anolyte, a constant N<sub>2</sub> flow was also used as a carrier gas, which mixed with gases released from catholyte, venting into the gas sampling-loop of the GC for periodical quantification, followed with an in situ volumetric flow meter (Figure S6). We found CO<sub>2</sub> gas released from the catholyte, along with only trace amount of H<sub>2</sub> in Figure 4. It should be noted that the mole ratio of CO<sub>2</sub>/H<sub>2</sub> released from the catholyte is 5000, which means that the purity of released CO<sub>2</sub> is about 99.98%.

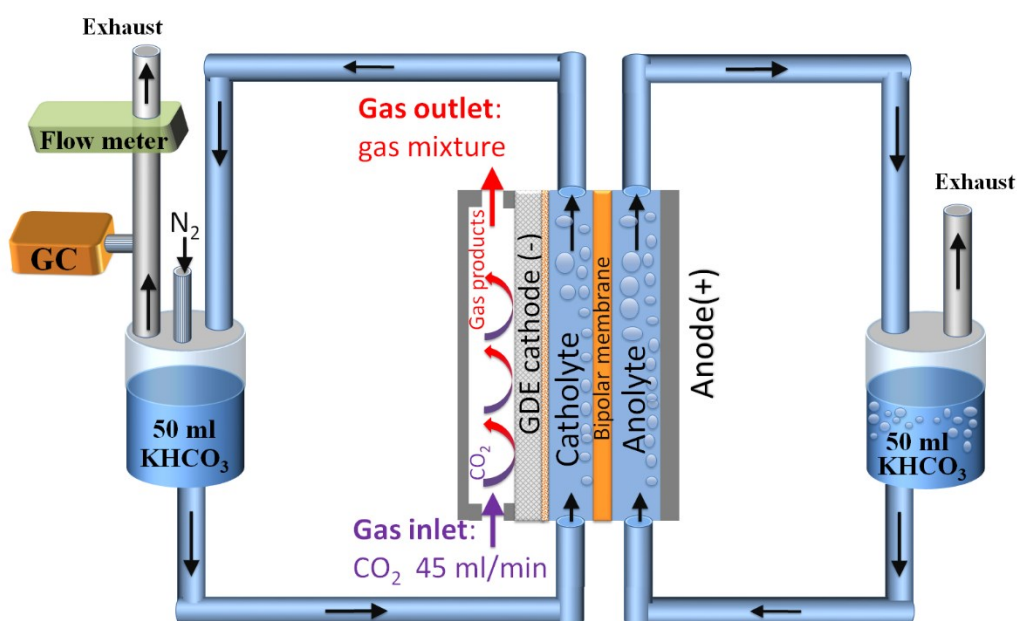


Figure S6. The schematic illustration of flow cell setup for detection of gases released from the catholyte over the course of  $\text{CO}_2$  reduction under the use of BPM. 1 M  $\text{KHCO}_3$  was used as initial catholyte (50 ml) and anolyte (50 ml).

### Applied potentials on the cathode

Potentiostatic electrochemical impedance spectroscopy (PEIS) was conducted on Cu deposited GDE in the flow electrolyzer to determine the solution resistance ( $R_s$ ). A detailed procedure was described in a previous work.<sup>5</sup> It should be noted that the distance between reference and cathode was less than 2 mm in order to reduce  $R_s$  in this work. Table S1 shows the solution resistance for the different ion-selective membranes. However, the cathodic reactions at high current densities can lead to a significant change of ion species and related concentration in the vicinity of the cathode, which indicates a difference in solution resistance near the cathode at high current densities compared to that of PEIS which was performed at relative low current densities. Thus, this difference in the solution resistance is closely correlated with the accuracy in IR-corrected potentials at a high current.

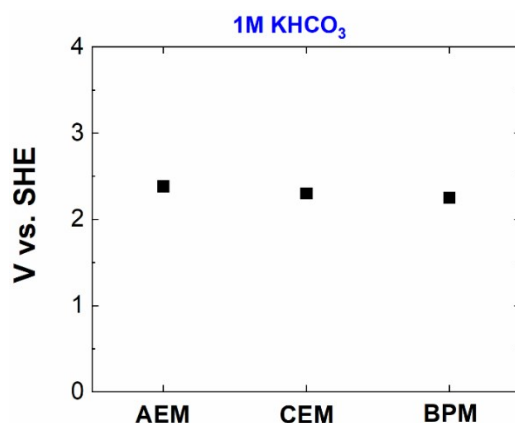


Figure S7. Applied potentials under the use of the different ion-selective membranes in 1 M  $\text{KHCO}_3$  aqueous solutions. (The potentials were not iR-corrected).

**Table S1.** IR-corrected potentials for  $\text{CO}_2$  reduction at  $200 \text{ mA/cm}^2$  in 1 M  $\text{KHCO}_3$  under the use of the different ion-selective membranes.

Membrane type	$R_s$ ( $\Omega$ )	Corrected V vs. SHE
AEM	1.375	-1.63
CEM	1.25	-1.60
BPM	1.38	-1.50

### Theoretical estimation of $\text{O}_2$ and $\text{CO}_2$ flowrate generated from electrolyte

Assuming that all charge passed through the anode is just employed for oxidation of water into  $\text{O}_2$ , thus theoretical  $\text{O}_2$  flowrate released from anolyte can be expressed as<sup>5</sup>:

$$\phi(\text{O}_2) = \frac{Q_{tot}}{nF} \times \frac{RT}{P_o} \quad (\text{S14})$$

where  $n$  and  $Q_{tot}$  are the number (here is 4) of electrons lost from 2  $\text{H}_2\text{O}$  for forming one  $\text{O}_2$  molecule and total charge passed through the anode, respectively.  $F$  is the faradaic constant,  $R$  is ideal gas constant,  $T$  is absolute temperature, and  $P_o$  is ambient pressure.

From our previous work, the ratio of  $\text{CO}_2$  and  $\text{O}_2$  released from the anolyte will be 4, 2 and 0 if the only anion species for neutralization reaction with  $\text{H}^+$  is  $\text{HCO}_3^-$ ,  $\text{CO}_3^{2-}$  or  $\text{OH}^-$ .<sup>5</sup> Thus, after

getting the O<sub>2</sub> flowrate at 200 mA/cm<sup>2</sup> (the cathode with 2 cm<sup>2</sup> geometric active area was used for all the tests) based on the equation S14, we can easily get the related flow of CO<sub>2</sub>, as shown in Table S2.

**Table S2.** The theoretically calculated flowrates of O<sub>2</sub> and CO<sub>2</sub> released from electrolyte if the only anion species for neutralization reaction with H<sup>+</sup> is HCO<sub>3</sub><sup>-</sup>, CO<sub>3</sub><sup>2-</sup> or OH<sup>-</sup> at 200 mA/cm<sup>2</sup>.

Anion species for neutralization with H <sup>+</sup>	CO <sub>2</sub> flow (ml/min)	O <sub>2</sub> flow (ml/min)
HCO <sub>3</sub> <sup>-</sup>	5.970	1.492
CO <sub>3</sub> <sup>2-</sup>	2.985	1.492
OH <sup>-</sup>	0	1.492

### Electrolyte pH and conductivity measurements

pH of the catholyte and the anolyte was monitored by a pH meter (pH 110, VWR) during the electrolysis. In addition, the pH meter was also equipped with a temperature sensor for the temperature-compensation. The pH meter was calibrated by a standard pH 7 buffer and a standard pH 10 buffer before the measurement.

The conductivity of the catholyte and the anolyte was monitored by a conductivity meter (PCE-PHD 1-PH, PCE Instruments) during CO<sub>2</sub> reduction electrolysis. Before the measurement, the conductivity meter was calibrated via conductivity standard of 1413 μS / cm (25 °C; 0.01 M KCl) and 111.8 mS / cm (25 °C; 1 M KCl) purchased from VWR. It should be noted that both of the calibration and the measurement were temperature-compensated due to that the solution conductivity is also temperature-dependent at a fixed solution concentration.

Because the AEMs are positively charged, anions can pass, and the crossover of positively charged ions will be decreased drastically.<sup>4</sup> In other words, no ideal AEM can absolutely avoid the crossover of positively charge ions. In this work, for the use of the AEM, when the anion species served as the main charge carriers transporting from the catholyte to the anolyte via the membrane, a small amount of  $K^+$  slowly crossed over from the anolyte to the catholyte via the AEM. Thus, the anolyte concentration gradually decreased, along with the correspondingly increased catholyte concentration over electrolysis, leading to the related variation in the anolyte and catholyte conductivity over time (Figure S8a).

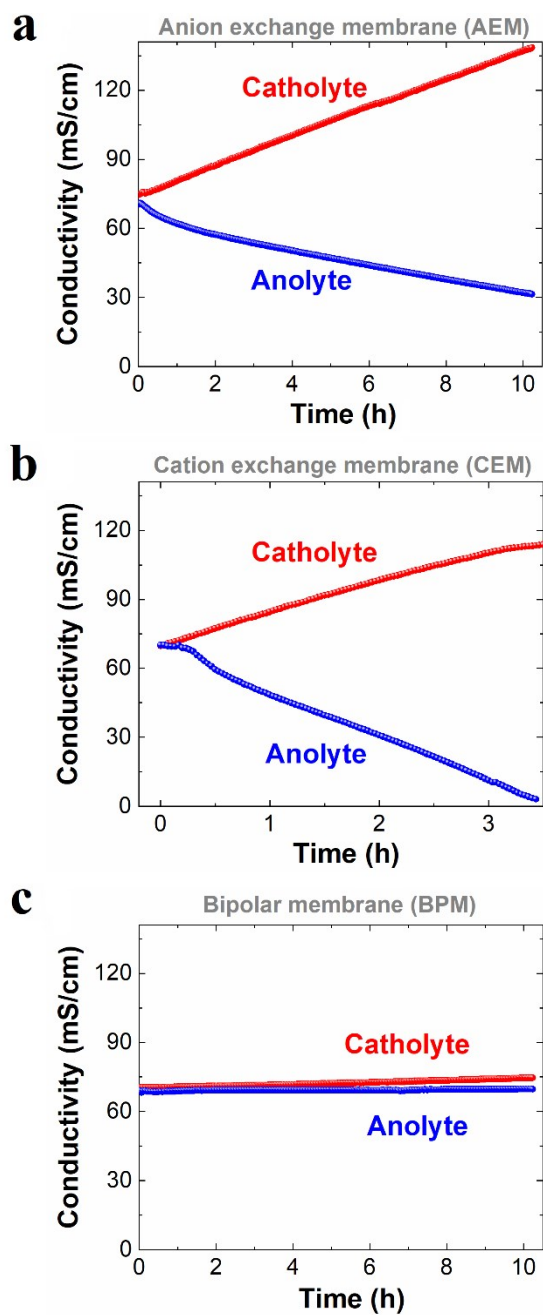


Figure S8. Conductivity of catholyte and anolyte as a function of time when using AEM (a), CEM (b) and BPM (c) over the course of CO<sub>2</sub> reduction electrolysis at 200 mA/cm<sup>2</sup>. 1 M KHCO<sub>3</sub> was used for both catholyte (50 ml) and anolyte (50 ml).

## Calculation of the carbon balance

The residual unreacted CO<sub>2</sub> flowrate in the gas outlet (gas mixture) out of gas compartment of flow electrolyzers can be written as:

$$\phi_{residual\ CO_2} = \phi_{outlet} - (\phi_{CO} + \phi_{CH_4} + \phi_{C_2H_4} + \phi_{H_2}) \quad (S15)$$

where  $\phi_{outlet}$  is the monitored gas flowrate out of the reactor during CO<sub>2</sub> reduction electrolysis using the setup shown in Figure 2S. Here,  $\phi_{CO}$ ,  $\phi_{CH_4}$ ,  $\phi_{C_2H_4}$  and  $\phi_{H_2}$  are the gas flowrate of CO, CH<sub>4</sub>, C<sub>2</sub>H<sub>4</sub> and H<sub>2</sub> produced from electrochemical CO<sub>2</sub> conversion in the gas outlet, respectively. Based on the equation S1-3, each molecule of CO, CH<sub>4</sub> and C<sub>2</sub>H<sub>4</sub> formation requires 1, 1 and 2 CO<sub>2</sub> molecule, Thus, the consumed CO<sub>2</sub> flowrate that is converted into all gas products (CO, C<sub>2</sub>H<sub>4</sub> and CH<sub>4</sub>) in CO<sub>2</sub> reduction can be expressed as below:

$$\phi_{CO_2\ to\ gas} = \phi_{CO} + \phi_{CH_4} + 2\phi_{C_2H_4} \quad (S16)$$

Depending on the number of carbon atoms in liquid molecule produced in CO<sub>2</sub> reduction, the consumed CO<sub>2</sub> flowrate involved in all liquid products formation can be written as:

$$\phi_{CO_2\ to\ liquid} = \phi_{C_1} + \phi_{C_2} + \phi_{C_3} \quad (S17)$$

where  $\phi_{C_1}$ ,  $\phi_{C_2}$ , and  $\phi_{C_3}$  are the consumed CO<sub>2</sub> flowrate for forming C<sub>1</sub>, C<sub>2</sub> and C<sub>3</sub> liquid products, respectively. For high-rate CO<sub>2</sub> reduction, the inevitably captured CO<sub>2</sub> in forms of carbonate via reaction with OH<sup>-</sup> could consume substantial CO<sub>2</sub> flow, significantly reducing the total gas flow out of the reactor (Figure 1c). It is known that the carbon element from CO<sub>2</sub> inlet flowrate should be eventually balanced with those of residual unreacted CO<sub>2</sub>, all products and carbonate formed via reaction between OH<sup>-</sup> and CO<sub>2</sub>. Thus, the consumed CO<sub>2</sub> flowrate via the reaction with OH<sup>-</sup> generated on the cathode surface can be expressed as:

$$\phi_{OH^-} = \phi_{inlet\ CO_2} - (\phi_{residual\ CO_2} + \phi_{CO_2\ to\ gas} + \phi_{CO_2\ to\ liquid}) \quad (S18)$$

where  $\phi_{inlet\ CO_2}$  is CO<sub>2</sub> flowrate fed into the gas chamber of the reactor. In this work, a constant CO<sub>2</sub> flow was used. It should be noted that mass flow controller used in this work was calibrated for CO<sub>2</sub> flow by volumetric flow meter before and after each CO<sub>2</sub> reduction test for high accuracy. Thus, we got the below carbon balance in Table S3.



**Table S3.** Carbon balance and related CO<sub>2</sub> utilization rate (ratio of CO<sub>2</sub> used in products formation versus total CO<sub>2</sub> consumption) for different ion-selective membranes in 1 M KHCO<sub>3</sub>.

Membrane type	$\Phi_{CO_2 \text{ to gas}}$ (ml/min)	$\Phi_{CO_2 \text{ to liquid}}$ (ml/min)	$\Phi_{OH^-}$ (ml/min)	$\Phi_{residual CO_2}$ (ml/min)	CO <sub>2</sub> utilization rate (%)
AEM	0.922	0.3917	2.74	41.02	~32.4
CEM	0.91885	0.391	2.75	40.99	~32.3
BPM	0.966	0.385	2.499	41.15	~35.1

( $\Phi_{CO_2 \text{ to gas}}$ : the consumed CO<sub>2</sub> flowrate that is converted into all gas products (CO, C<sub>2</sub>H<sub>4</sub> and CH<sub>4</sub>) in CO<sub>2</sub> reduction;  $\Phi_{CO_2 \text{ to liquid}}$ : the consumed CO<sub>2</sub> flowrate for all liquid products in CO<sub>2</sub> reduction (such as ethanol);  $\Phi_{OH^-}$ : the consumed CO<sub>2</sub> flowrate via the reaction with OH<sup>-</sup> generated in cathodic reactions;  $\Phi_{residual CO_2}$ : the residual unreacted CO<sub>2</sub> flowrate in the gas outlet (gas mixture) out of gas compartment of flow electrolyzers)

### Correlation between the carbonate/bicarbonate ratio and pH

The pH of a buffer solution can be estimated by the Henderson–Hasselbalch equation, as below:

$$pH = pK_a + \log_{10}\left(\frac{[CO_3^{2-}]}{[HCO_3^-]}\right) \quad (S19)$$

where pKa is the acid dissociation constant, and  $[CO_3^{2-}]/[HCO_3^-]$  is the concentration ratio of  $CO_3^{2-}$  to  $HCO_3^-$ . The above equation can be rewritten as:

$$\frac{[CO_3^{2-}]}{[HCO_3^-]} = 10^{(pH - pK_a)} \quad (S20)$$

Here, the pKa is 10.3 at 25 °C based on the equation S9. The pH of the catholyte was measured by the pH meter for the different membranes, as shown in Figure 3d, e and f. Thus, the concentration ratio of carbonate/bicarbonate in the catholyte can be estimated according to the equation S20. Table S4 shows the typical concentration ratio of carbonate to bicarbonate at different pH values. Before starting the electrolysis, the initial 1 M  $KHCO_3$  has a pH value of ~8.3, which corresponds to  $[CO_3^{2-}]/[HCO_3^-]$  ratio of 0.01. For the AEM, the pH is ~11.33 after ~10 h (Figure 3d), corresponding to  $[CO_3^{2-}]/[HCO_3^-]$  ratio of 10, which is consistent with the catholyte transformation from bicarbonate to carbonate over the electrolysis. For the BPM, the catholyte pH was maintained < 9 over the entire electrolysis (Figure 3f), indicating that most of anion species was bicarbonate.

**Table S4.** The calculated ratio of  $[CO_3^{2-}]/[HCO_3^-]$  at typical catholyte pH values.

pH	$[CO_3^{2-}]/[HCO_3^-]$ ratio
~8.3	0.01
~9	0.05
~10	1
~11.33	10

### **Cell voltage**

Cell voltage as a function of time when using the three different membranes over the course of CO<sub>2</sub> reduction electrolysis is shown in Figure S9, which indicates that an additional potential of ~ 2 V was required for the BPM compared to those of the use of CEM and AEM. In addition, it should be noted that an apparent fluctuation in the applied potentials was observed due to the effect of CO<sub>2</sub> degassing at the BPM/catholyte interface. With the use of the CEM, the anolyte conductivity rapidly decreased from ~70 mS/cm to ~3 mS/cm after ~ 3 h (Figure S8b), which leads to the increased cell voltages for maintaining the constant current density of 200 mA/cm<sup>2</sup> (Figure S9b).

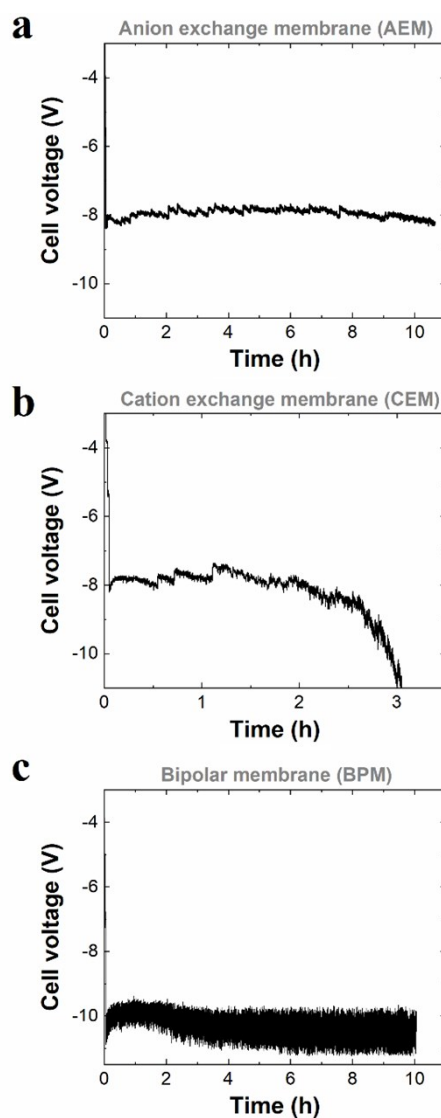


Figure S9. Cell voltage as a function of time when using AEM (a), CEM (b) and BPM (c) over the course of CO<sub>2</sub> reduction electrolysis at 200 mA/cm<sup>2</sup>. 1 M KHCO<sub>3</sub> was used for both catholyte (50 ml) and anolyte (50 ml). The distance between the Cu cathode and the membrane was ~15 mm.

## REFERENCES

- 1 K. P. Kuhl, T. Hatsukade, E. R. Cave, D. N. Abram, J. Kibsgaard and T. F. Jaramillo, *Journal of the American Chemical Society*, 2014, **136**, 14107–14113.
- 2 Y. Hori, in *Modern Aspects of Electrochemistry*, ed. E. Vayenas, C. G., White, R. E., Gamboa-Aldeco, M. E., Springer New York, New York, NY, 2004, vol. 70, pp. 89–189.
- 3 M. Ma, K. Djanashvili and W. A. Smith, *Angewandte Chemie International Edition*, 2016, **55**, 6680–6684.
- 4 K. P. Kuhl, E. R. Cave, D. N. Abram and T. F. Jaramillo, *Energy & Environmental Science*, 2012, **5**, 7050.

- 5 M. Ma, E. L. Clark, K. T. Therkildsen, S. Dalsgaard, I. Chorkendorff and B. Seger, *Energy & Environmental Science*, 2020, **3**, 977–985.